



# Observations of the late 1980s regime shift in the Earth's climate system

James Foster, NASA GSFC Code 617

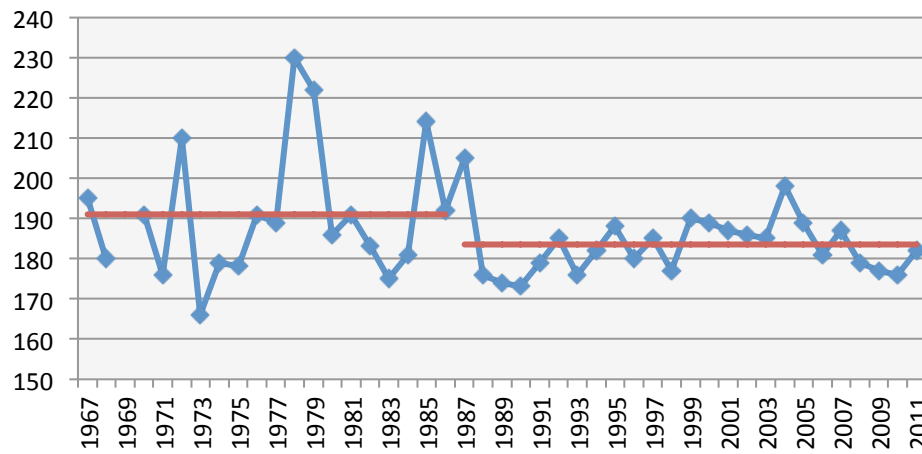


Figure 1: First Snow Free Day (70N, 110 W)

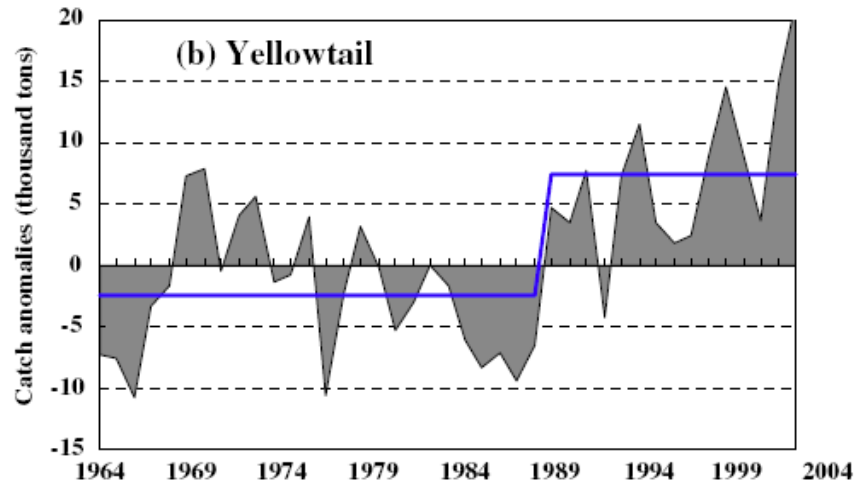


Figure 3: Fish catch Sea in Japan/Eastern Sea

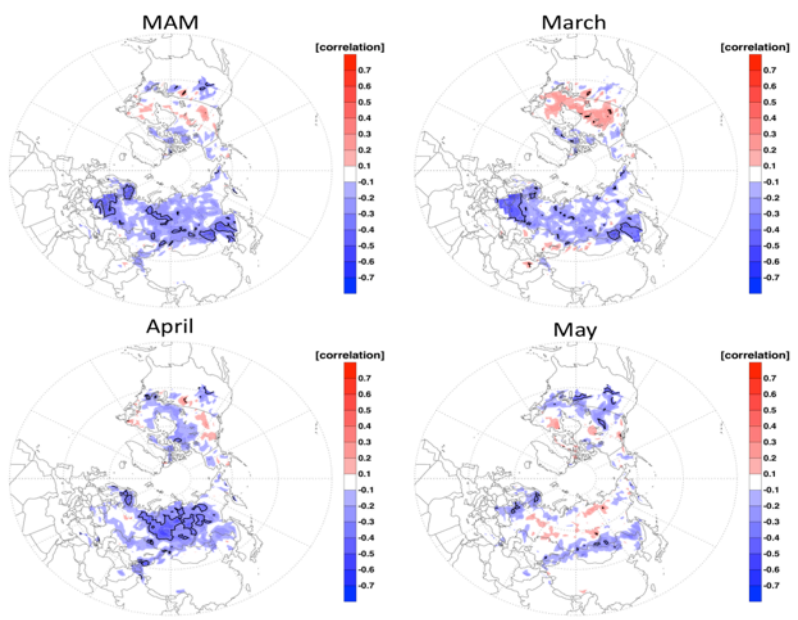


Figure 2: Correlation of final week snow cover with M-M AO, for the years 1973-2011. The 95% significance level is contoured in black.

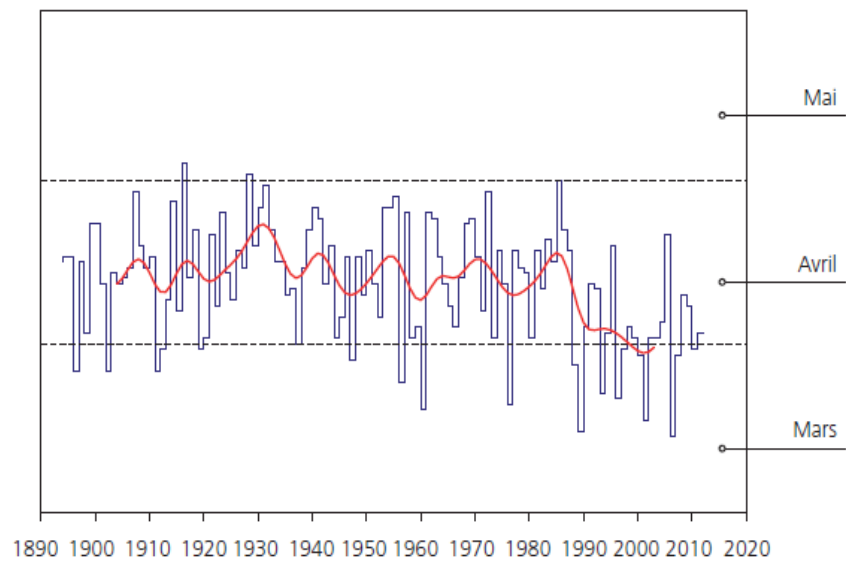


Figure 4: Cherry blossom: date of flowering at Liestal, Switzerland



**Name: James Foster, NASA/GSFC, Code 617**

**E-mail: [james.l.foster@nasa.gov](mailto:james.l.foster@nasa.gov), Phone: 301-614-5769**

**Abstract:**

Regime shifts reflect sudden and substantial change in the state of a system; three have occurred in the last few decades ~1976, ~1987 and ~1997, with the greatest documented evidence so far from ~1987. In agreement with this observation, spring snow cover across Arctic lands has, on average, retreated approximately five days earlier since the late 1980s compared to the previous twenty years. However, it appears that since about the late 1980s, the date the snowline first retreats north during the spring has changed only slightly -- in the last twenty years or so the date of snow disappearance has not been occurring significantly earlier. Meaningful correlations between the Arctic Oscillation (AO) during both the winter and spring seasons and the date of snowmelt have been identified. When the springtime (AO) is strongly positive, snow tends to melt out earlier.

**References:**

Philip C. Reid, Renata E. Hari, Grégory Beaugrand, David M. Livingston, Christoph Marty, Dietmar Straile, Pierre Helaout, Rita Adrian, Ross Brown, **James Foster**, and 11 others: "The late 1980s regime shift in the Earth's climate system and its global impacts" (in preparation).

**Foster, JL**, J Cohen, DA Robinson, and TW Estilow: 2008, "A look at the date of snowmelt and correlations with the Arctic Oscillation," *Annals of Glaciology* (accepted for publication), 2013.

**Data Sources:**

NOAA visible/infrared satellite data (snow maps).

**Technical Description of Figures:**

**Figure 1:** First Snow Free Day for years 1967-2011 (70N, 110 W)

**Figure 2:** Correlation of final week snow cover with March-May AO, for the years 1973-2011. The 95% significance level contoured in black.

**Figure 3:** Yellowtail tuna catch in Sea of Japan -- *Tian, Y., H. Kidokoro, T. Watanabe, and N. Iguchi: 2008, "The late 1980s regime shift in the ecosystem of Tsushima warm current in the Japan/East Sea: Evidence from historical data and possible mechanisms," Progress in Oceanography, Vol. 77, 127-145.*

**Figure 4:** Cherry blossom: date of flowering Liestal, Switzerland – *Meteo-Swiss Report on the year 2011*

**Scientific significance:**

The ~1987 shift was first outlined for terrestrial and marine plants and subsequently for a range of biotic, physical and chemical variables in terrestrial, lacustrine, riverine, oceanic, and cryospheric systems. In the Japan/East Sea, for example, an abrupt change from cooling to warming occurred in the late 1980s, particularly in the Tsushima warm current region. Many, but not all, biological components of the ecosystem, from plankton to predatory fishes, and including both warm-water pelagic species (such as yellowtail tuna) and cold-water species responded to the sharp shift. Elsewhere, warming in Switzerland after about 1986 has prompted earlier blooming of cherry trees. In regards to the cryosphere, snowmelt changes observed since the late 1980s have been step-like in nature, unlike a more continuous downward trend seen in Arctic sea ice extent. When the springtime (AO) is strongly positive, snow will melt out earlier. When the springtime AO is strongly negative, snow disappears later in the spring. The winter AO and snowmelt relationship is not as straightforward.

**Relevance for future science and relationship to Decadal Survey:**

The timing of climate changes, across a number of different physical systems, is likely forced by a threshold increase in temperature, the source of which may be a shift in AO and related higher sea surface temperatures.



# Reducing Land Surface Model Uncertainty with Remotely Sensed Surface Soil Moisture

Ken Harrison, ESSIC/Code 617, Sujay Kumar, SAIC/Code 617, Christa Peters-Lidard, Code 617,  
and Joe Santanello, Code 617, NASA GSFC

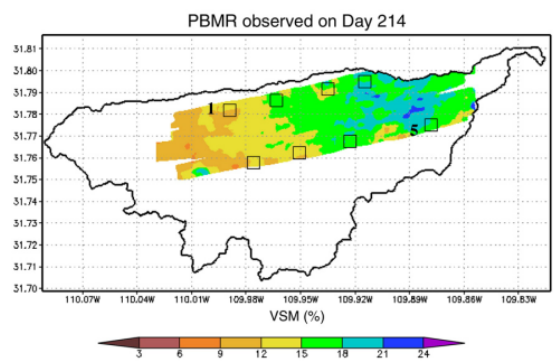


**Figure 1:** The heavily instrumented sites 1 and 5 of the Walnut Gulch Experimental Watershed in Arizona were the focus of this study. The remote sensing data consisted of surface soil moisture estimates derived from airborne measurements from the NASA push broom microwave radiometer (PBMR) flown for the Monsoon '90 Experiment.

Highest  
Probability  
Zero

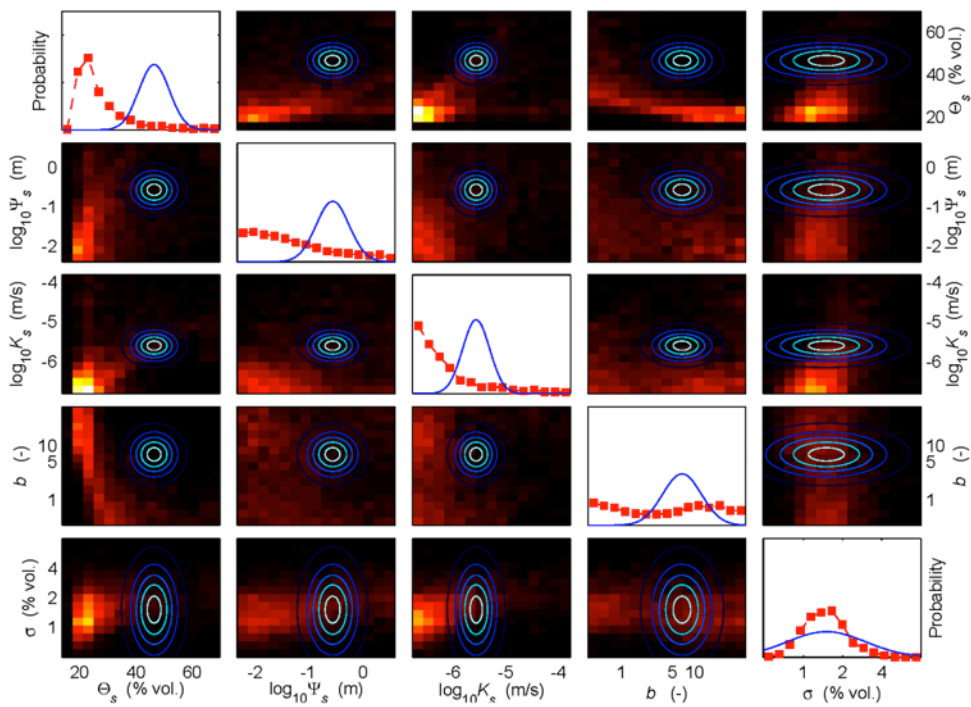


**Figure 2:** The uncertainty in soil hydraulic properties at site 5 as initially assessed from soil texture lookup tables (blue), and as updated with the PBMR remote sensing data (red). The shift in the probability distribution for each individual parameter is shown along the diagonal. The shift in the joint probability distribution for each pairing of parameters is shown in the off-diagonal plots, with the blue contours representing the “prior” and the image the “posterior”.

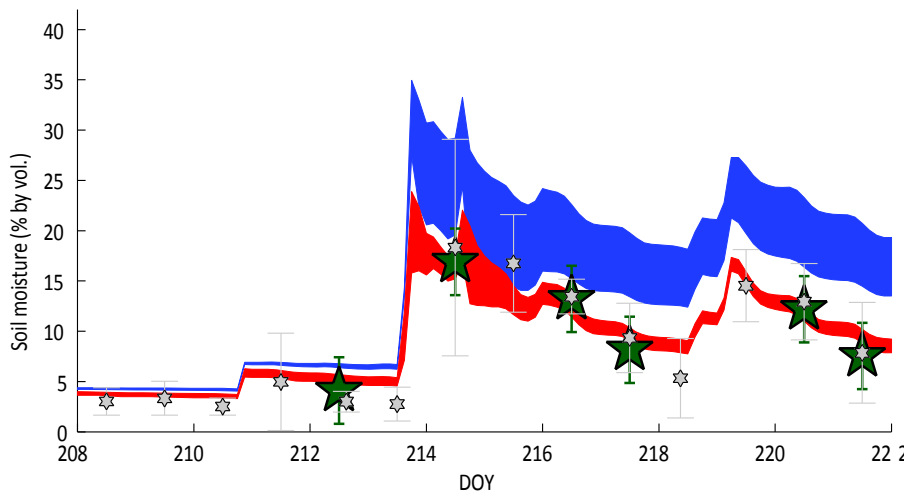


**Figure 3:** Prior (blue) and posterior (red) estimates of the uncertainty in surface soil moisture at site 5. The shaded areas encompass the true surface soil moisture with two-thirds probability. The posterior estimates are more consistent with the PBMR (green) and *in situ* gravimetric (gray) observations .



Name: Ken Harrison, ESSIC, NASA/GSFC, Code 617

E-mail: ken.harrison@nasa.gov

Phone: 301-286-7095

### Abstract:

This work presents the first application of a new uncertainty estimation capability of the NASA Land Information System (LIS) that draws on novel, recently developed Bayesian statistical algorithms. For a site in the Walnut Gulch Experimental Watershed in Arizona, the impact of airborne L-band remote sensing data on soil hydraulic property and soil moisture simulation uncertainty is evaluated.

### References:

Harrison, K. W., S. V. Kumar, C. D. Peters-Lidard, and J. A. Santanello (2012), "Quantifying the change in soil moisture modeling uncertainty from remote sensing observations using Bayesian inference techniques", *Water Resources Research*, 48, W11514, doi:10.1029/2012WR012337

**Data Sources:** Monsoon '90 experiment datasets as described in Kustas and Goodrich (1994) [Kustas, W. P., and D. C. Goodrich (1994), Preface [to special section on Monsoon '90 Multidisciplinary Experiment], *Water Resour. Res.*, 30(5), 1211–1225, doi:10.1029/93WR03068]. Airborne L-band observations as detailed in Schmugge et al. (1994) [Schmugge, T., T. J. Jackson, W. P. Kustas, R. Roberts, R. Parry, D. C. Goodrich, S. A. Amer, and M. A. Wetz (1994), Push broom microwave radiometer observations of surface soil-moisture in monsoon 90, *Water Resour. Res.*, 30(5), 1321–1327.]

### Technical Description of Figures:

**Figure 1:** This site map shows the location (latitude and longitude) of the Walnut Gulch Experimental Watershed, along with the locations of the instrumented sites (black boxes) and the PBMR data (colored swath) collected on day 214 (August 2) of 1990.

**Figure 2:** Prior and posterior marginal probability distributions of the soil hydraulic properties that include the saturated matric potential ( $\psi_s$ ), the saturated hydraulic conductivity ( $K_s$ ), the saturated soil moisture content (porosity;  $\theta$ ), and the pore size distribution index ( $b$ ); an error term ( $\sigma$ ) representing model/observation error is also included. The contours for the prior on the off-diagonal plots represent 10%, 30%, 50%, 70%, and 90% of maximum marginal prior probability density. Note that these marginal plots are windows into the un-viewable full 5-dimensional space.

**Figure 3:** The prior and posterior simulated soil moisture time series. The range is defined by the 17<sup>th</sup> and 83<sup>rd</sup> percentiles, as assessed through application of Monte Carlo methods (prior: standard Monte Carlo; posterior: Markov chain Monte Carlo using the Differential Evolution Markov Chain method). The range represents the uncertainty stemming from the soil hydraulic property uncertainty (Figure 2).

### Scientific significance:

Soil hydraulic parameters, which are spatially variable and scale-dependent, are a large source of land surface modeling uncertainty. As in situ data are unavailable at global modeling scales, operational land surface models generally rely on soil texture class-based lookup table mean estimates. This approach, however, ignores the large variability of soils within the same soil texture class. In prior work, we have applied remote sensing to infer best estimates of soil hydraulic properties at appropriate modeling scales. Here, we extend this work by quantifying the uncertainty in soil hydraulic properties and the resultant uncertainty in the simulation of soil moisture.

### Relevance for future science and relationship to Decadal Survey:

Many applications, including hydrologic applications (e.g., flooding, droughts, landslides), rely on Level 4 (model-generated) data products. As risk is typically a major factor in these applications, it is important to accurately report the uncertainty in the data products. Second, the reduction in modeling uncertainty, here land surface modeling uncertainty, enabled with observing systems is an important measure of mission worth. Finally, it is important for allocating scientific resources to better understand the uncertainties of the models and their inputs.





# Taking stock of circumboreal forest carbon with spaceborne LiDAR

Christopher Rudasill-Neigh, Code 618, NASA/GSFC

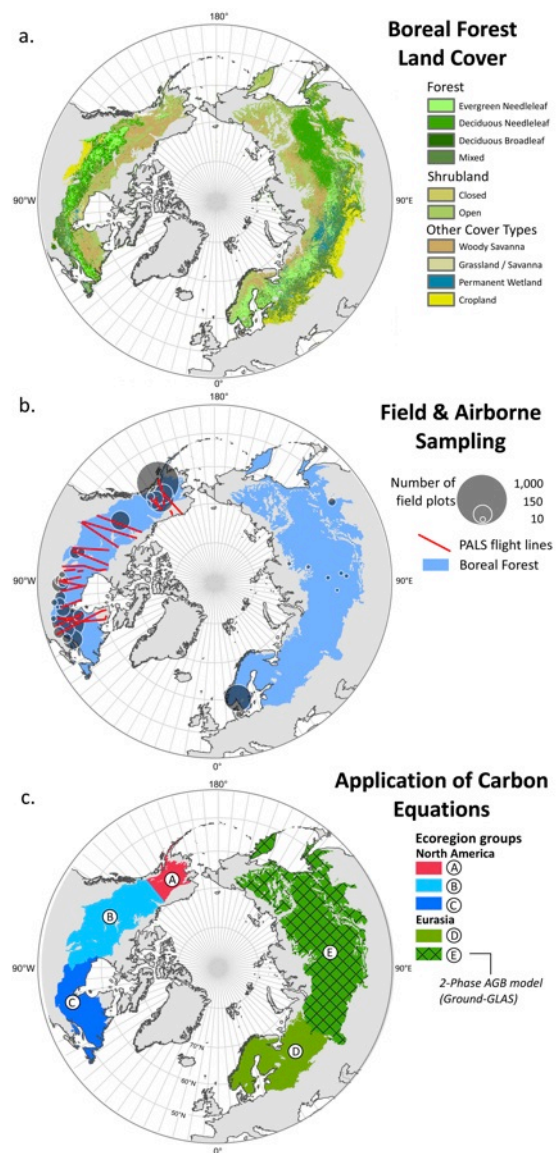


**Figure 1.** Methods. a. MODIS land cover stratification. b. Biomass sampling density. c. Ecoregion stratification of biomass models applied.

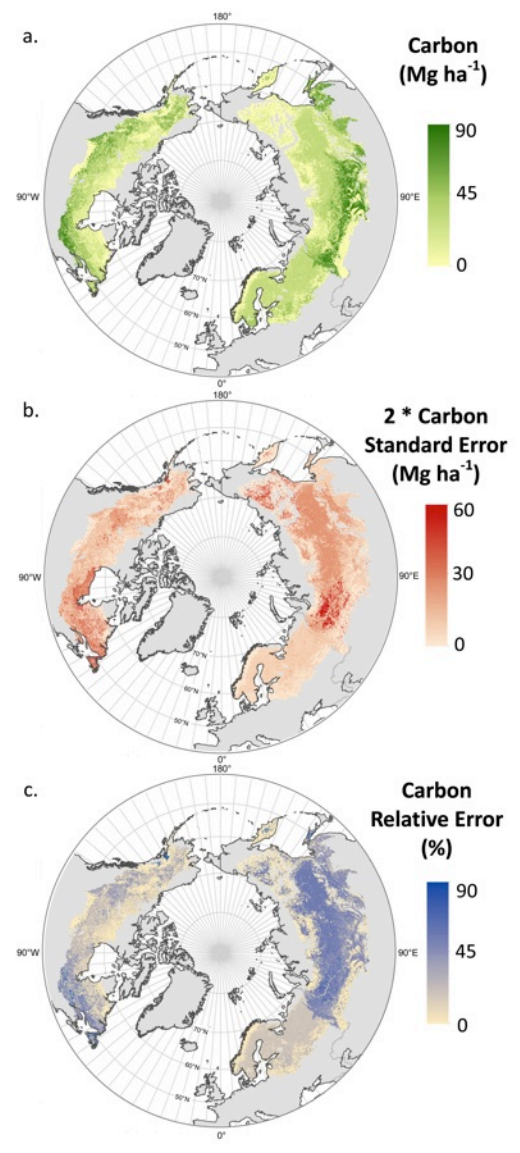


**Figure 2.** Results. a. Aboveground carbon. b. and c. Error estimates of carbon density.



**Name:** Christopher Rudasill-Neigh, Code 618, NASA/GSFC  
**E-mail:** Christopher.S.Neigh@nasa.gov  
**Phone:** 301-614-6681

#### **Abstract:**

The boreal forest accounts for one-third of global forests, but is largely inaccessible to measurements of carbon stock. We derived the first satellite-based map of aboveground carbon, with errors, for the entire biome. Physically meaningful forest structure information can be retrieved from ICESat GLAS waveforms and correlated to field and airborne LiDAR measurements.

#### **References:**

- 2013 Neigh C.S.R., Nelson R.F., Ranson K.J., Margolis H., Montesano P., Sun G., Kharuk V., Næsset E., Wulder M.A., and Andersen H.E. Taking stock of circumboreal forest carbon with spaceborne LiDAR. *Remote Sensing of Environment*. Submitted 01/25/13.
- 2011 Ranson, K.J., Montesano, P.M., Nelson, R.F. Object Mapping the circumpolar taiga-tundra transition zone with MODIS tree cover. *Remote Sensing of Environment*. 115, Pages: 3670–3680.
- 2011 Guoqing S., Kimes D., Forest biomass mapping from lidar and radar synergies. *Remote Sensing of Environment*. 115, Pages: 2906-2916 DESDynI VEG-3D Special Issue.
- 2009 Montesano P.M., Nelson R., Sun G., Margolis H., Kerber A., Ranson, K. J. MODIS tree cover validation for the circumpolar taiga-tundra transition zone. *Remote Sensing of Environment*. 113, Pages: 2130-2141.
- 2009 Nelson R., Ranson K.J., Sun G, Kimes D.S., Kharuk V., Montesano P.M. Estimating Siberian timber volume using MODIS and ICESat/GLAS. *Remote Sensing of Environment*. 113, Pages: 691-701.
- 2008 Boudreau J.; Nelson Ross F.; Margolis Hank A.; et al. Regional aboveground forest biomass using airborne and spaceborne LiDAR in Quebec. *Remote Sensing of Environment*. 112, Pages: 3876-2008.

**Data Sources:** This was a joint effort composed of multiple international agencies and universities including the US Forest Service (forest inventory data, Figure 1b), Canadian Forest Service (forest inventory data), Russian Academy of Sciences (forest inventory data), Norwegian University of Life Sciences (Airborne ALTM LiDAR and forest inventory data), NASA-GSFC (Landsat and MODIS Figure 1a, land cover products and burned area, ASTER GDEM Global Digital Elevation Model V1, Airborne PALS LiDAR, Figure 1b), University of Maryland (ICESat Ice Cloud and Land Elevation satellite, GLAS Geoscience Laser Altimeter System waveform metrics), and the University of Laval (Airborne PALS LiDAR).

#### **Technical Description of Images:**

**Figure 1.** Circumboreal forest stratification. a. Land cover information derived from MODIS and produced in the International Geosphere Biosphere Program classification scheme. b. The map shows the biomass sampling density throughout the study area with number of field plots shown by the size of grey circles. Red depicts portable airborne laser system (PALS) flight lines over co-located GLAS waveforms. c. A color-coded map depicting the regional spatial stratification of biomass models applied.

**Figure 2.** Circumboreal forest results. a, Aboveground carbon. b,c Error estimates of carbon density. The images illustrate stratum-level estimates.

**Scientific significance:** The spatial distribution of aboveground forest carbon is poorly known over many areas of the globe. Estimates of forest carbon are required for accurate prediction and modeling of changes in carbon sinks and sources. This work is the first to demonstrate for the entire boreal forest how remotely sensed data on forest structure combined with modeling may be used to infer total aboveground carbon stock and distribution with estimates of error.

**Relevance for future science and relationship to Decadal Survey:** Forest carbon is a critical component of the carbon cycle, and is sensitive to climate change and disturbances. The boreal forest has experienced large increases in warming and is expected to warm the most of all forest biomes. Forest structure observations from the ICESat and ICESat 2 to be launched early 2016 timeframe, combined with airborne and field measurements, will provide the necessary data products to infer aboveground carbon stock in forests worldwide using the techniques presented in this work.



# Use of in situ and airborne multiangle data to assess MODIS- and Landsat-based estimates of directional reflectance and albedo

Miguel O. Román, Code 619, NASA/GSFC

CAR-30m, Landsat, and MODIS vs. CART Site (DOY 153-155, 2007)

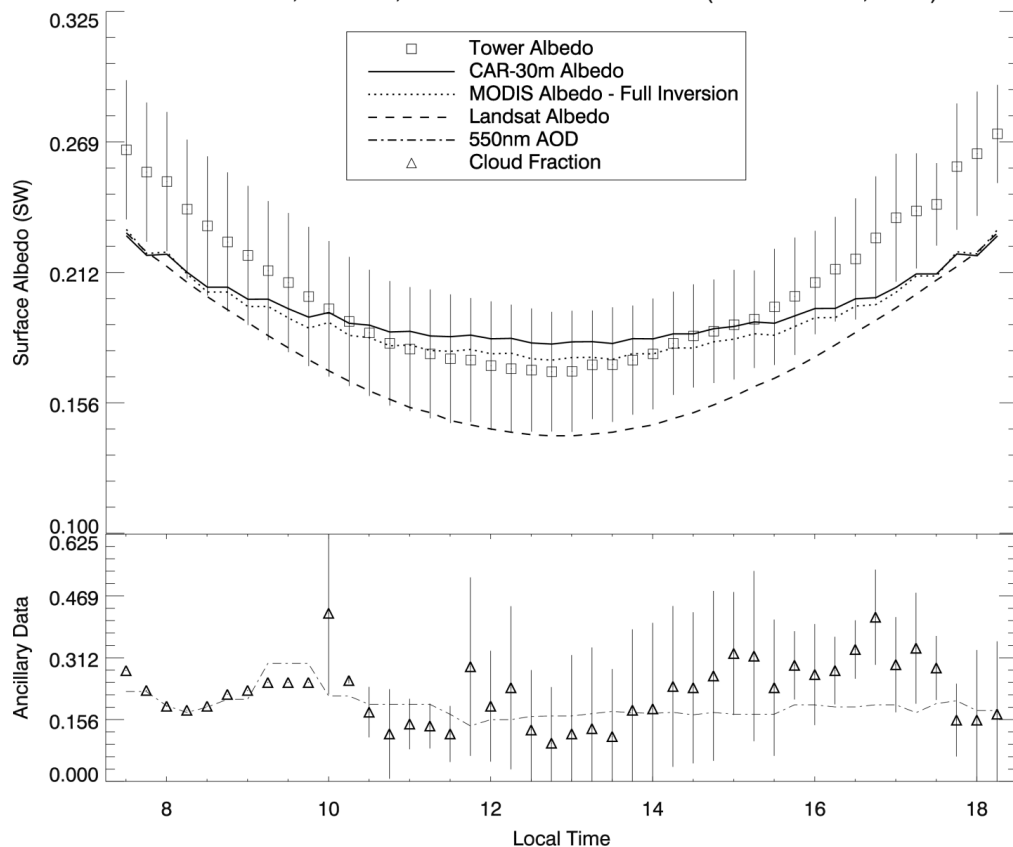
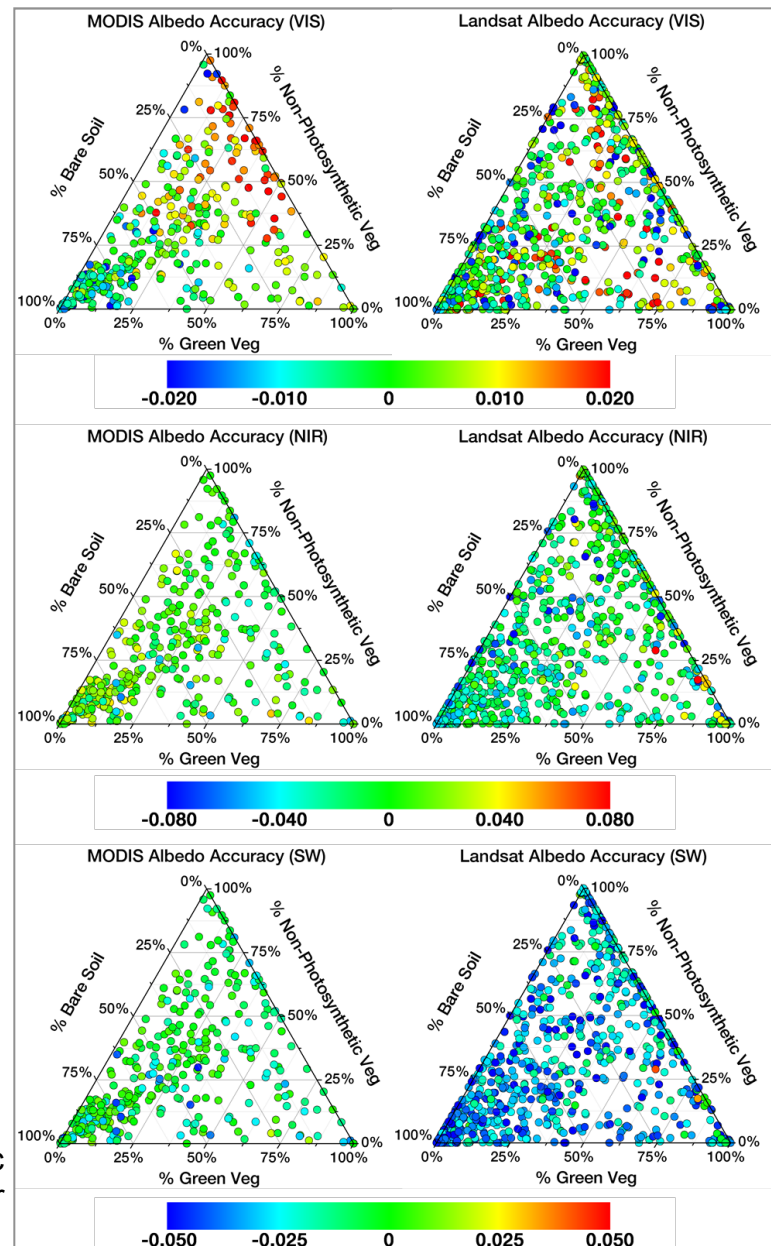


**Figure 1:** Comparisons between surface albedos derived from CAR, MODIS, Landsat-TM, and tower-based measurements acquired at the Atmospheric Radiation Measurement Cloud and Radiation Testbed (ARM/CART) site in northern Oklahoma.

**Figure 2:** Ternary diagrams illustrating the pixel-specific accuracy of MODIS- and Landsat-derived albedos for a 10km x 10km region centered on the ARM/CART site.





Name: Miguel Román, NASA/GSFC, Code 619  
E-mail: [Miguel.O.Roman@nasa.gov](mailto:Miguel.O.Roman@nasa.gov)  
Phone: 301-614-5498

## Abstract:

This work presents the results from a multiscale assessment of MODIS and Landsat-TM albedo retrievals based on collocated comparisons with tower and airborne Cloud Absorption Radiometer (CAR) measurements obtained during the 2007 Cloud and Land Surface Interaction Campaign (CLASIC'07) over the Atmospheric Radiation Measurement (ARM) Cloud and Radiation Testbed (ARM/CART) in Oklahoma, USA.

## References:

Román, M.O., Gatebe, C.K., Shuai, Y., Wang, Z., Gao, F., Masek, J.G., He, T., Liang, S., & Schaaf, C.B. (2013). Use of in situ and airborne multiangle data to assess MODIS- and Landsat-based estimates of directional reflectance and surface albedo. *IEEE Transactions on Geoscience and Remote Sensing: Special Issue on Inter-Calibration of Satellite Instruments*, doi:10.1109/TGRS.2013.2243457.

**Data Sources:** This is a joint effort between [NASA-GSFC's Terrestrial Information Systems Laboratory](#) (algorithm development and validation efforts), [NASA-GSFC's Climate and Radiation Laboratory](#) (CAR data acquisition and processing), and the [University of Massachusetts Boston](#) (MODIS BRDF/albedo data). CAR airborne datasets over the Atmospheric Radiation Measurement Program's (ARM) Southern Great Plains (SGP) Cloud and Radiation Testbed (CART) site in Oklahoma, USA (available at <http://car.gsfc.nasa.gov/data/>) were acquired with support from NASA's Science Mission Directorate as part of the Earth Observing System (EOS) Radiation Sciences Program and Airborne Science Program (NASA Grants NNX08AF89G, NNX07AT35H, and NNX08AE94A); and the U.S. Department of Energy (DOE-DE-FG02-06ER64178).

## Technical Description of Figures:

**Figure 1:** Comparisons between instantaneous retrievals of surface albedo acquired at the ARM/CART site, accompanied by coincident measurements of aerosol optical depth and cloud fraction.

**Figure 2:** Ternary diagrams illustrating the pixel-specific accuracy of MODIS and Landsat shortwave albedos (Satellite – Airborne) for a 10 km x 10 km region centered on the ARM/CART tower. Results are expressed in terms of three major fractional cover types: % green vegetation, % non-photosynthetic vegetation (NPV), and % bare soils. To determine the composition of a point within the triangular area, a series of three lines can be drawn through the point of interest, with each line parallel to a side of the triangle. With these lines in place, the percentage of each fractional cover type can be determined and drawn as a function of satellite retrieval accuracy (MODIS on the left-hand side and Landsat on the right-hand side).

## Scientific significance:

The quantification of uncertainty in satellite-derived global surface albedo products is a critical aspect in producing complete, physically consistent, and decadal land property data records for studying ecosystem change. The methodology presented in this paper addresses a major challenge in validating albedo measurements acquired from space, by overcoming the spatial scaling errors that can produce disagreements between satellite and field-measured values.

## Relevance for future science and relationship to Decadal Survey:

With its unique design (190°swath, 1°IFOV, oversampling every 0.5° along the vertical plane) and unparalleled instrument accuracy ( $\leq 5\%$ ), NASA's Cloud Absorption Radiometer (CAR) provides accurate representations of different ecosystem types across a broad range of retrieval scenarios. This capability is being used by different instrument science teams (e.g., MODIS, Landsat, and S-NPP VIIRS) in support of global product validation and intercomparison studies, as well as for research efforts that necessitate reference datasets of uniform quality to monitor instrument performance and assess product quality.